Proceedings Paper:
Alshaya, A, Nie, L orcid.org/0000-0002-5796-907X, Cowell, DMJ orcid.org/0000-0003-0854-542X et al. (3 more authors) (2019) Monitoring Needle Biopsy of Sentinel Lymph Nodes Using Photoacoustic Image with Dynamic-FDMAS Beamformer. In: Proceedings of the 2019 IEEE International Ultrasonics Symposium (IUS). 2019 IEEE International Ultrasonics Symposium (IUS), 06-09 Oct 2019, Glasgow, United Kingdom. IEEE , pp. 490-493. ISBN 978-1-7281-4597-6

https://doi.org/10.1109/ultsym.2019.8926274

Monitoring Needle Biopsy of Sentinel Lymph Nodes Using Photoacoustic Image with Dynamic-FDMAS Beamformer

Abdulrhman Alshaya*†, Luzhen Nie *, David M. J. Cowell*,T. Carpenter *, James R. McLaughlan*‡, and Steven Freear*

*Ultrasonics and Instrumentation Group, School of Electronic and Electrical Engineering, University of Leeds, Leeds, LS2 9JT, UK.

†King Abdulaziz City for Science and Technology (KACST), Riyadh, Saudi Arabia

‡Leeds Institute of Cancer and Pathology, School of Medicine, University of Leeds, Leeds, LS9 7TF, UK.

E-mail: aaalshaya@kacst.edu.sa and S.Freear@leeds.ac.uk

***Abstract*—As a part of the diagnosis pathway for breast cancer, a needle biopsy of the sentinel lymph node (SLN) is taken for analysis. Photoacoustic imaging is a better approach for guide a needle than ultrasound imaging. However, the photoacoustic image will be affected by clutter, phase aberration and artefact from the needle. In this study, dynamic filter delay multiply and sum (D-FDMAS) beamformer was produced to reduce these effects and improve the SNR and contrast difference (CD) of imaging targets. D-FDMAS beamformer with 16 elements sub-group size (16 D-FDMAS) showed improvement in SNR of needle and inclusion (SLN) by 8.38 dB and 5.42 dB compared with delay and sum (DAS) beamfomer. It also showed reduction in CD between inclusion and needle by almost 12 dB compared with filter delay multiply and sum (FDMAS) beamformer.**

I. Introduction

A breast cancer is one of the common cancers that women suffer from. It is a reason of death more than 0.5 million women in 2012 [1], [2]. An early detection of breast cancer will lead to increase the percentage of the survive rate [3], [4]. A part of the diagnosis pathway for breast cancer, a needle biopsy of the sentinel lymph node (SLN) is taken for analysis. When ultrasound imaging is used, it will be difficult to differentiate between SLN and other lymph nodes [5]. Therefore, researchers investigate photoacoustic imaging to guided the needle. In photoacoustic imaging, exogenous contrast agents such as indocyanine green (ICG) are injected near to the tumour. This contrast agent that has a narrow optical absorption spectrum is propagated in the lymphatic system. As a result, the location of SLN is defined by generated photoacoustic image for this contrast agent [5], [6].

In photoacoustic imaging, clutter, phase aberration and directivity of the transducer affected on the image equality. These effects are high if delay and sum (DAS) beamformer that is the most popular in photoacoustic imaging is used. In this beamformer, the spatial resolution is reduced and side-lobes and artefact are generated [7]–[9]. Researchers have used some advance beamforming techniques to reduce these effect such as filter delay multiply and sum (FDMAS) beamformer [10], [11]. This beamfoerming technique shows improvement in spatial resolution and reduction in side-lobes. However, the correlation operation in the FDMAS beamformer affect on the contrast difference (CD) between different targets such as SLN and needle.

In this study, dynamic filter delay multiply and sum (D-FDMAS) beamformer was produced to reduce these effects and improve signal to noise ratio (SNR), spatial resolution and contrast of the photoacoustic image. D-FDMAS beamformer will be compared with DAS and FDMAS beamformers in terms of SNR and CD based on needle experiments.

II. Method

A. Dynamic Filter Delay Multiply and Sum (D-FDMAS) Beamforming technique

D-FDMAS beamformer depends on correlation operation between a delayed RF-signal of sub-group of transducer elements. This is unlike FDMAS beamformer that depends on correlation opeation between the delayed RF-signal of all transducer elements. The ideal of D-FDMAS is taken from the sub-FDMAS beamformer [11]. However, In the D-FDMAS beamformer, the delayed RF-signal for each transducer element is correlated with itself to emphasize the energy of beamformed data as given in Eq.1:

$$y_{D-FDMAS} = \{\sum_{i=1}^{N}\sum_{j=i}^{m} sign(S_i(t)S_j(t)).\sqrt{|S_i(t)S_j(t)|}\} * f$$

$$m = \begin{cases} i+L-1 & L \leq N-i \\ N & else \end{cases} \tag{1}$$

where N is the number of transducer elements, $S_i(t)S_j(t)$ is the delayed RF-signal for element i and j respectively, L is the sub-group size of elements, $sign$ is the sign operation to save the phase of signal after multiplication and f is band pass filter to remove the low frequency part of the signals. In this beamformer, the delayed RF-signal for each transducer element is correlated with itself to emphasize the energy of the beamformed data that have been applied before by Su *et al.* [12]. The multiplication number of D-FDMAS beamformer is calculated by using Eq.2:

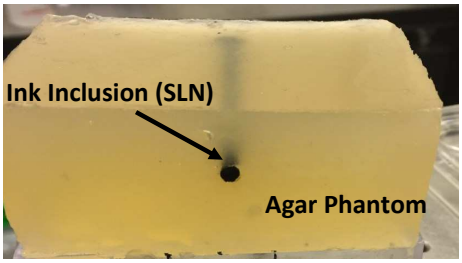

Fig. 1: The agar phantom with ink inclusion (SLN).

$$NU_{D-FDMAS} = LN - (\frac{L^2 - L}{2}) \quad (2)$$

III. Experiment Setup

In this experiment, An agar phantom with inclusion was used as shown in Fig.1. The recipe of the agar phantom was taken from [13], [14]. The same recipe was used for the inclusion excipt the agar material was not used and 20 % Indian ink (Dr.Ph.Martins, Black Star) was used as absorbent material. This inclusion was used as SLN. The depth of this inclusion was around 1.2 cm. A needle (Blunt Fill Needle, 18G) was inserted inside the phantom to generate photoacoustic emissions from the needle and inclusion simultaneously. The setup of this experiment is shown in Fig.2. Nd-YAG laser was used to fire laser pulses on the phantoms. This pulses was guided to the phantom through optical fibre that had one input and seven outputs (BF76LS01, Thorlabs). The wavelenght and the energy per pulse were 850 nm and 3.7 mJ respectively. The generated photoacoustic emissions were recorded by using Ultrasound Array Research Platform II (UARP II) [15]–[18] with 128 elements linear transducer (Verasonics L11-4). The center frequency and bandwidth (-6 dB) of the linear transducer were 7 MHZ and (4 to 11) MHz respectively. These received photoacoustic emissions were averaged 100 times before beamforming them. The data was analysed based on SNR and CD after beamforming with the DAS, FDMAS and D-FDMAS beamformers.

IV. Result and Discussion

The received photoacoustic emissions were beamformed by using D-FDMAS with different sub-group size as shown in Fig.3. The background noise and needle artefact were reduced as the sub-group size was increased. However, the CD between needle and inclusion was increased when the sub-group size was increased. The SNR and CD of the inclusion and needle were calculated for different sub-group size. The SNR was calculated by using Eq.3 [19]:

$$SNR = 20\log_{10}(\frac{\mu_{Signal}}{\sigma_{Backgound}}) \quad (3)$$

where μ_{Signal} is the mean of the signal and $\sigma_{Backgound}$ is the standard deviation of the background noise. In Fig.3

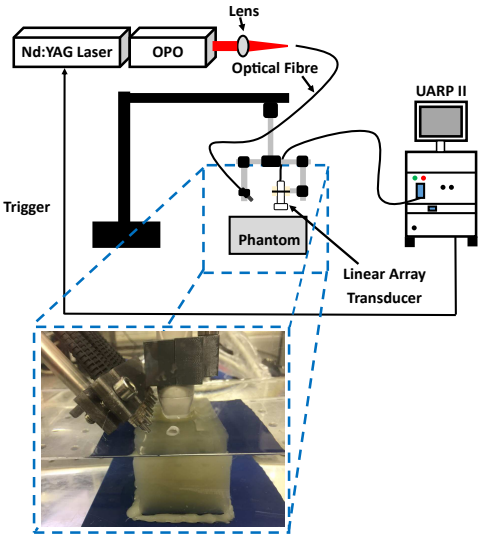

Fig. 2: The experiment setup.

(A), the solid rectangular number 1 and 2 were the signal and background noise regions for the needle respectively. The dashed rectangular number 1 and 2 were the signal and background noise regions for inclusion respectively. Table.I shows the SNR of photoacoustic images beamformed by using D-FDMAS with different sub-group size. The contrast ratio (CR) was calculated by using Eq.4 [20]:

$$CR = 20\log_{10}(\frac{\mu_{Signal}}{\mu_{Backgound}}) \quad (4)$$

where $\mu_{Backgound}$ is the mean of the background. In Fig.3 (A), the solid rectangular number 1 and the dashed rectangular number 1 are the signal regions of needle and inclusion respectively. The solid rectangular number 2 is the background region. Table.II shows the CD between needle and inclusion when photoacoustic images beamformed by using D-FDMAS with different sub-group size. From Table. I and Table. II, The highest SNR of the needle was 26.29 dB when the sub-group size was 16 elements. The SNR of the inclusion was improved as the sub-group size was increased. However, the CD between inclusion and needle was increased as the sub-group size was increased. For instance, when sub-group size was 4 elements, the CD was 0.52. This CD was increased to 13.78 dB when the sub-group size was 128 elements. By using 16 D-FDMAS and 32 D-FDMAS, the CD was 2.23 dB and 7.89 dB respectively. These CD do not effect recognizing inclusion and needle as shown in Figs. 3 (C) and (D).

The 16 D-FDMAS beamformer was compared with the DAS and FDMAS beamformer as shown in Fig. 4. Fig.4 (A) shows ultrasound image for inclusion and needle. This ultrasound image was generated from single plane wave. The contrast of the needle was low. Fig.4 (B) shows photoacoustic image for the needle and inclusion when the DAS beamformer was used. In this photoacoustic image, the background noise is high. There are also high artefact from the needle. When the FDMAS beamformer is used as shown in Fig.4 (C), the

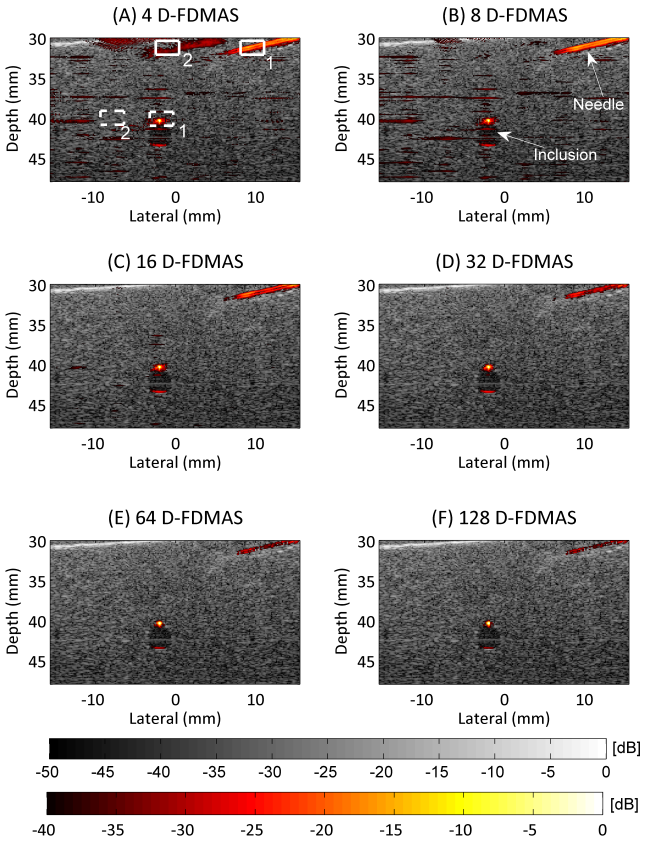

Fig. 3: Photoacoustic images for inclusion and needle when the D-FDMAS beamformer with different sub-group were used. (A) 4 elements, (B) 8 elements, (C) 16 elements, (D) 32 elements, (E) 64 elements and (F) 128 elements. In all photoacoustic images (Hot colormap), ultrasound image (Gray colormap) was use as background image. The dynamic range for ultrasound and photoacoustic images are 50 dB and 40 dB respectively.

TABLE I: SNR of photoacoustic image beamformed by using D-FDMAS with different sub-group size.

D-FDMAS	SNR (dB)	
Sub-group	Inclusion	Needle
4	25.86	21.14
8	27.52	25.4
16	32.17	26.29
32	36.03	21.71
64	42.04	21.05
128	43.47	21.13

background noise and needle artefact are significantly reduced. However, the CD between needle and inclusion was increased. This will affect recognizing the needle. This is because the difference shape of the propagation RF-signals between needle and inclusion. The SNR and CD of the inclusion and needle

TABLE II: CR of photoacoustic image beamformed by using D-FDMAS with different sub-group size.

D-FDMAS	Contrast Ratio (dB)		
Sub-group	Inclusion	Needle	Difference
4	15.01	15.53	0.52
8	17.79	18.79	1.00
16	22.41	20.18	2.23
32	26.11	18.23	7.89
64	30.27	17.74	12.52
128	31.52	17.74	13.78

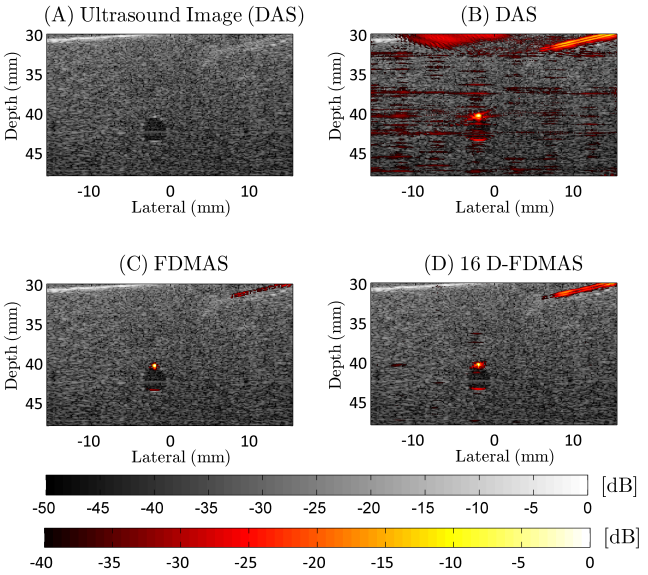

Fig. 4: Ultrasound and photoacoustic image for inclusion and needle. (A) Ultrasound image, (B) photoacoustic image with DAS, (C) photoacoustic image with FDMAS and (D) photoacoustic image with 16 D-FDMAS. In all photoacoustic image, ultrasound image was used as background. The dynamic range for ultrasound and photoacoustic images are 50 dB and 40 dB respectively.

were calculated by using the same step that is used in the D-FDMAS beamformer. Table. III and Table. IV show the SNR and CD when using DAS, FDMAS and 16 D-FDMAS. From Table.III and Table.IV, FDMAS beamformer improved SNR of the needle and inclusion by 3 dB and 17.44 dB respectively compared with DAS beamformer. However, the CD between needle and inclusion was increased by almost 13 dB. This create difficulties to recognize and track needle as shown in Fig.4 (C). The 16 D-FDMAS beamformer (Fig.4 (D)) improved the SNR of inclusion and needle by 5.42 dB and 8.38 dB respectively compared with DAS the beamformer. In addition, it reduced the CD by almost 12 dB compared with the FDMAS beamformer.

The number of multiplication of D-FDMAS depends on the sub-group size. When the number of transducer elements is 128, the optimum sub-group size was between 16 and 32 elements. From Eq.2, when the sub-group size is 32 elements,

TABLE III: SNR of the photoacoustic images.

	SNR (dB)	
Beamformer	**Inclusion**	**Needle**
DAS	26.75	17.91
FDMAS	44.19	20.95
16 D-FDMAS	32.17	26.29

TABLE IV: CR of the photoacoustic images.

	Contrast Ratio (dB)		
Beamformer	**Inclusion**	**Needle**	**Difference**
DAS	10.82	9.85	0.97
FDMAS	31.53	17.41	14.12
16 D-FDMAS	22.41	20.18	2.23

the number of multiplication is 3600 times. whereas, when the FDMAS beamformer is used, the number of multiplication is 8128 times. The reduction of multiplication number that the D-FDMAS beamformer achieved make it more suitable for real time imaging when it is processed by using GPU processor.

V. Conclusion

In this paper, D-FDMAS beamformer was produced. The optimum sub-group size was between 16 and 32 elements. By using D-FDMAS with 16 sub-group elements, the CD was significantly reduced compared with FDMAS beamformer. The SNR of needle and inclusion enhanced by 8.38 dB and 5.42 dB respectively compared with DAS beamformer. In addition, the computation time of D-FDMAS beamfomer is much less than that of FDMAS beamfomer. In future work, D-FDMAS will be processed by using GPU and applied in real time imaging.

References

[1] M. I. Nounou, F. ElAmrawy, N. Ahmed, K. Abdelraouf, S. Goda, and H. Syed-Sha-Qhattal, "Breast cancer: conventional diagnosis and treatment modalities and recent patents and technologies," *Breast cancer: basic and clinical research*, vol. 9, pp. BCBCR–S29 420, 2015.

[2] M. Heijblom, D. Piras, M. Brinkhuis, J. C. van Hespen, F. Van den Engh, M. Van der Schaaf, J. Klaase, T. Van Leeuwen, W. Steenbergen, and S. Manohar, "Photoacoustic image patterns of breast carcinoma and comparisons with magnetic resonance imaging and vascular stained histopathology," *Scientific reports*, vol. 5, p. 11778, 2015.

[3] S. Zackrisson, S. Van De Ven, and S. Gambhir, "Light in and sound out: emerging translational strategies for photoacoustic imaging," *Cancer research*, vol. 74, no. 4, pp. 979–1004, 2014.

[4] M. Mehrmohammadi, S. Joon Yoon, D. Yeager, and S. Y Emelianov, "Photoacoustic imaging for cancer detection and staging," *Current molecular imaging*, vol. 2, no. 1, pp. 89–105, 2013.

[5] K. Sivasubramanian, V. Periyasamy, and M. Pramanik, "Non-invasive sentinel lymph node mapping and needle guidance using clinical handheld photoacoustic imaging system in small animal," *Journal of biophotonics*, vol. 11, no. 1, p. e201700061, 2018.

[6] C. Kim, T. N. Erpelding, K. I. Maslov, L. Jankovic, W. J. Akers, L. Song, S. Achilefu, J. A. Margenthaler, M. D. Pashley, and L. V. Wang, "Handheld array-based photoacoustic probe for guiding needle biopsy of sentinel lymph nodes," *Journal of biomedical optics*, vol. 15, no. 4, p. 046010, 2010.

[7] E. J. Alles, M. Jaeger, and J. C. Bamber, "Photoacoustic clutter reduction using short-lag spatial coherence weighted imaging," in *Ultrasonics Symposium (IUS), 2014 IEEE International*. IEEE, 2014, pp. 41–44.

[8] S. Park, S. Mallidi, A. B. Karpiouk, S. Aglyamov, and S. Y. Emelianov, "Photoacoustic imaging using array transducer," in *Photons Plus Ultrasound: Imaging and Sensing 2007: The Eighth Conference on Biomedical Thermoacoustics, Optoacoustics, and Acousto-optics*, vol. 6437. International Society for Optics and Photonics, 2007, p. 643714.

[9] S. Park, A. B. Karpiouk, S. R. Aglyamov, and S. Y. Emelianov, "Adaptive beamforming for photoacoustic imaging," *Optics letters*, vol. 33, no. 12, pp. 1291–1293, 2008.

[10] G. Matrone, A. S. Savoia, G. Caliano, and G. Magenes, "The delay multiply and sum beamforming algorithm in ultrasound b-mode medical imaging," *IEEE transactions on medical imaging*, vol. 34, no. 4, pp. 940–949, 2015.

[11] A. Alshaya, S. Harput, A. M. Moubark, D. M. J. Cowell, J. McLaughlan, and S. Freear, "Spatial resolution and contrast enhancement in photoacoustic imaging with filter delay multiply and sum beamforming technique," in *2016 IEEE International Ultrasonics Symposium (IUS)*, Sept 2016, pp. 1–4.

[12] T. Su, D. Li, and S. Zhang, "An efficient subarray average delay multiply and sum beamformer algorithm in ultrasound imaging," *Ultrasonics*, vol. 84, pp. 411–420, 2018.

[13] L. Nie, S. Harput, D. M. J. Cowell, T. M. Carpenter, J. R. Mclaughlan, and S. Freear, "Combining acoustic trapping with plane wave imaging for localized microbubble accumulation in large vessels," *IEEE Transactions on Ultrasonics, Ferroelectrics, and Frequency Control*, vol. 65, no. 7, pp. 1193–1204, July 2018.

[14] J. Browne, K. Ramnarine, A. Watson, and P. Hoskins, "Assessment of the acoustic properties of common tissue-mimicking test phantoms," *Ultrasound in medicine & biology*, vol. 29, no. 7, pp. 1053–1060, 2003.

[15] P. R. Smith, "Ultrasonic phased array techniques using switched-mode excitation," Ph.D. Thesis, University of Leeds, UK, 2013.

[16] D. M. J. Cowell, P. R. Smith, and S. Freear, "Phase-inversion-based selective harmonic elimination (PI-SHE) in multi-level switched-mode tone- and frequency- modulated excitation," *Ultrasonics, Ferroelectrics and Frequency Control, IEEE Transactions on*, vol. 60, no. 6, pp. 1084–1097, 2013.

[17] P. R. Smith, D. M. J. Cowell, B. Raiton, C. V. Ky, and S. Freear, "Ultrasound array transmitter architecture with high timing resolution using embedded phase-locked loops," *Ultrasonics, Ferroelectrics and Frequency Control, IEEE Transactions on*, vol. 59, no. 1, pp. 40–49, 2012.

[18] S. Harput, "Use of chirps in medical ultrasound imaging," Ph.D. Thesis, School of Electronic and Electrical Engineering, University of Leeds, UK, 2012.

[19] D. Wang, Y. Wang, W. Wang, D. Luo, U. Chitgupi, J. Geng, Y. Zhou, L. Wang, J. F. Lovell, and J. Xia, "Deep tissue photoacoustic computed tomography with a fast and compact laser system," *Biomed. Opt. Express*, vol. 8, no. 1, pp. 112–123, Jan 2017. [Online]. Available: http://www.osapublishing.org/boe/abstract.cfm?URI=boe-8-1-112

[20] S. M. Hverven, O. M. H. Rindal, A. Rodriguez-Molares, and A. Austeng, "The influence of speckle statistics on contrast metrics in ultrasound imaging," in *Ultrasonics Symposium (IUS), 2017 IEEE International*. IEEE, 2017, pp. 1–4.